THE JOURNAL OF PHYSICAL CHEMISTRY C

Article

pubs.acs.org/JPCC

Selective Functionalization of Halloysite Cavity by Click Reaction: Structured Filler for Enhancing Mechanical Properties of Bionanocomposite Films

Francesca Arcudi,[†] Giuseppe Cavallaro,[‡] Giuseppe Lazzara,*[,‡] Marina Massaro,[†] Stefana Milioto,[‡] Renato Noto,[†] and Serena Riela*[,†]

[†]Dipartimento STEBICEF, Sezione di Chimica, and [‡]Dipartimento di Fisica e Chimica, Università degli Studi di Palermo, Viale delle Scienze, Edificio 17, 90128 Palermo, Italy

Supporting Information

ABSTRACT: Selective modification of the inner surface of halloysite nanotubes (HNTs) by the cycloaddition of azides and alkynes (click reaction) was successfully achieved. Fourier transform infrared spectroscopy and thermogravimetry confirmed that the modification involved only the HNT cavity. Morphological investigations evidenced that the functionalized nanotubes formed microfibers and clusters in the micrometer range. By means of the casting method, these nanomaterials were dispersed into biopolymeric matrixes (chitosan and hydroxypropyl cellulose) with the aim of obtaining nanocomposite films with tunable properties from the physicochemical viewpoint. For comparison purposes, we also characterized composite nanomaterials based on pristine halloysite. The mesoscopic structure of the nanocomposites was correlated with their tensile, thermal, and wettability properties, which were found to be strongly dependent on both the nature of the polymer and the HNT functionalization. The attained knowledge represents a basic point for designing new hybrid nanostructures that are useful in specific purposes such as biocompatible packaging.

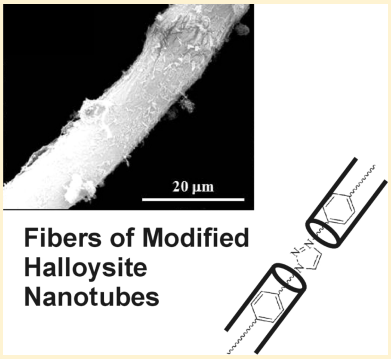

INTRODUCTION

The functionalization of clay nanoparticles represents a well-known technique for designing ecocompatible materials of technological interest. Among nanoclays, halloysite nanoparticles (HNTs) are very appealing because of their biocompatibility and versatile characteristics, such as large surface area, tunable surface chemistry, and hollow tubular morphology.[1,2] All of these features make HNTs suitable for use in catalyst supports,[3−6] water decontamination,[7,8] encapsulation and controlled release of chemically and biologically active compounds with smart functions (antibacterial,[9,10] anticorrosion,[11] and self-healing[12] functionalities), and fillers for polymers.[13−16]

HNTs are rather polydisperse in size with external diameters of 50−80 nm, lumens of 10−15 nm, and lengths of about 1000 nm.[1] The inner surface consists of a gibbsite octahedral sheet (Al−OH) groups, whereas the external surface is composed of siloxane groups (Si−O−Si). This peculiarity determines a positively charged lumen and a negatively charged outer surface in the pH range[2] between 2 and 8 that is responsible for pH-induced gel formation.[17]

Selective modification of HNT surfaces enable the control of both the aqueous colloidal stability and the adsorption capacity of the nanoparticles.[18] Functionalization of the HNT cavity with octadecylphosphonic acid[19] and sodium alkanoates[18] generates inorganic tubular micelles that can behave as sponges for hydrophobic molecules. On the other hand, modification of the HNT external surface can generate valuable catalyst supports, as demonstrated for metalloporphyrin immobilization[5] and the Suzuki coupling reaction.[4]

The hydrophilicity of both the inner and outer surfaces makes HNTs dispersible in aqueous biopolyelectrolytes such as pectin[14] and chitosan.[20] The combination between polymers and HNTs is a good strategy to develop nanocomposite films with desirable mechanical performance that can be utilized as biocompatible packaging[13,14,21] and as scaffolds for tissue engineering.[16] Filling hydroxypropyl cellulose (HPC) with HNTs was found to cause an increase in the polymer degradation temperature.[13] Pectin/HNT composite is thermally more stable than the pristine polymer, and the nanomaterial presents a uniform morphology.[14] A pectin/poly(ethylene glycol) (PEG) blend filled with HNTs was found to show better elastic properties than both the pristine polymers and the corresponding pectin/HNT nanocomposites.[22] The tensile strength and elastic modulus of chitosan are enhanced by HNTs at low filler loadings (up to 10 wt % filler content).[23] Nanoparticle functionalization is a well-established strategy for improving the compatibility and dispersibility of an inorganic filler in a polymer matrix.

Received: May 5, 2014
Revised: June 10, 2014

   dx.doi.org/10.1021/jp504388e | J. Phys. Chem. C XXXX, XXX, XXX−XXX

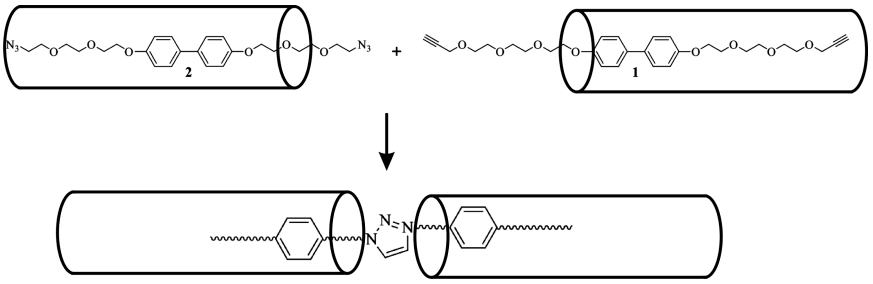

Figure 1. Schematic representation of the f-HNT synthesis.

In this work, the effect of functionalization of the inner surface of HNTs by the click reaction was investigated. For this purpose, we designed new molecules that can interact with both the internal surface of HNTs and each other through suitable terminal groups. The efficiency and selectivity of the reaction were estimated. Moreover, the morphology of the functionalized nanotubes was studied. The obtained materials were used as nanofillers for the development of nanocomposite films based on biopolymers. The bionanocomposites were extensively characterized from the physicochemical viewpoint by determining the mechanical properties, thermal degradation, and wettability. The acquired knowledge represents a basic point for designing new green nanomaterials.

EXPERIMENTAL METHODS

Materials. Chitosan (75−85% deacetylated, MW = 50−190 kg mol^{-1}) and HPC (MW = 80 kg mol^{-1}) were obtained from Aldrich. HNT was a gift from Applied Minerals, Inc. All reagents needed for HNT functionalization were purchased from Aldrich. All these materials were used without further purification.

Functionalization of Halloysite. The synthesis of functionalized halloysite nanoparticles (f-HNTs) was done by the click reaction, through the use of Cu^{2+}-catalyzed Huisgen 1,3-dipolar cycloaddition. Details on the syntheses of compounds **1** and **2** are given in the Supporting Information. A schematic of the synthesized molecules is shown in Figure 1. To functionalize the internal surface of halloysite, we placed each compound in the presence of halloysite in a ^{t}BuOH/water (1:1) for 48 h at room temperature in such a way that the encapsulation of **1** and **2** in the HNT lumen was facilitated.

Finally, dispersions of HNT/**1** and of HNT/**2** were mixed in the presence of a catalytic amount of $CuSO_4$ and sodium ascorbate for 7 days at room temperature to allow the click reaction between the azides and alkyne terminations of the different moieties from the inner HNT lumen. This was done with the aim of generating organized structures through the formation of functionalized HNT (f-HNT) (Figure 1).

Preparation of Nanocomposite Films. Nanocomposite films were prepared using the aqueous casting method as described elsewhere.[13] Briefly, we prepared a 2 wt % aqueous biopolymer (chitosan and HPC) solution under stirring at 70 °C. Then, an appropriate amount of filler (functionalized or pristine HNTs) was added to the biopolymer solution and kept under stirring overnight. The well-dispersed aqueous mixture was poured into glass Petri dishes at 60 °C to evaporate water until the weight was constant and to obtain biofilms with a thickness of ca. 0.12 mm. Dried biofilms contained 5 wt % nanofiller.

Instrumentation. *Thermogravimetry.* Thermogravimetry experiments were performed by means of a Q5000 IR apparatus (TA Instruments) under a nitrogen flow of 25 cm^3 min^{-1} for the sample and 10 cm^3 min^{-1} for the balance. The weight of each sample was ca. 10 mg. The temperature calibration was carried out by means of the Curie temperatures of standards (nickel, cobalt, and their alloys). The measurements were conducted by heating the sample from room temperature to 900 °C at a rate of 20 °C min^{-1}.

Scanning Electron Microscopy. The morphologies of the nanocomposites were studied using an ESEM FEI QUANTA 200F microscope. Before each experiment, the surface of the sample was coated with gold in argon by means of an Edwards Sputter Coater S150A to avoid charging under electron beam treatment. The measurements were carried out in high-vacuum mode (<6 × 10^{-4} Pa) for simultaneous secondary electrons. The energy of the beam was 20 kV, and the working distance was 10 mm. Minimal electron dose conditions were employed to avoid damaging the sample.

Fourier Transform Infrared (FTIR) Spectroscopy. FTIR spectra in KBr were determined at room temperature in the spectral region 400−4000 cm^{-1} by means of an FTIR spectrophotometer (Agilent Technologies Cary 630). An average of 30 scans per sample using a nominal resolution of 4 cm^{-1} was registered.

Dynamic Mechanical Analysis. Tensile properties were determined by means of a DMA Q800 instrument (TA Instruments). For all mechanical measurements, the samples were films of rectangular shape (10.00 mm × 6.00 mm × 0.120 mm). Tensile tests were performed with a stress ramp of 1 MPa min^{-1} at 26.0 ± 0.5 °C. We determined the values of the elastic modulus, the tensile strength (defined as the tensile stress at which the material fractures), and the elongation at the breaking point. Each nanocomposite was measured five times, and the average values are reported. Note that the films composed of chitosan did not undergo breakage even upon application of the largest force (18 N) allowed by the instrument.

Contact Angle Equipment. Contact angle studies were performed by means of an optical contact angle apparatus (OCA 20, Data Physics Instruments) equipped with a video measuring system having a high-resolution CCD camera and a high-performance digitizing adapter. SCA 20 software (Data Physics Instruments) was used for data acquisition. The water contact angle just after deposition was measured by the sessile drop method by gently placing a droplet of 6.0 ± 0.5 μL onto the surface of the film. The temperature was set at 25.0 ± 0.1 °C for the support and the injecting syringe as well. A minimum of five droplets were examined for each film sample. Only the chitosan-based films were analyzed.

dx.doi.org/10.1021/jp504388e | J. Phys. Chem. C XXXX, XXX, XXX−XXX

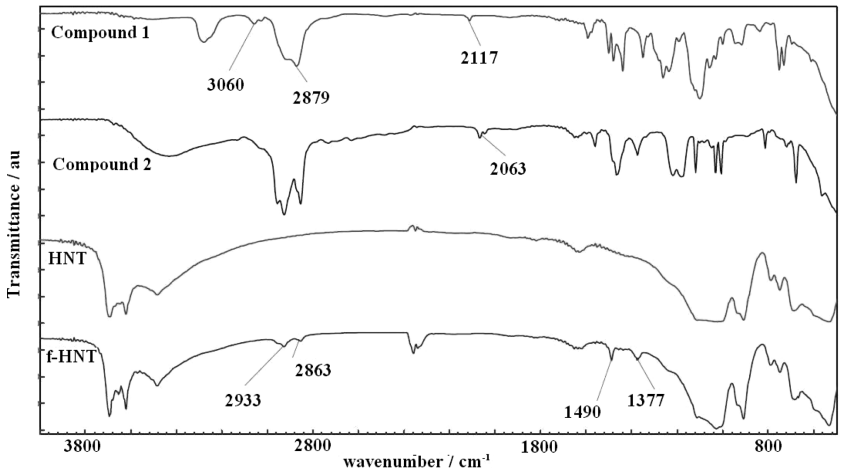

Figure 2. FTIR spectra of compound **1**, compound **2**, HNT, and f-HNT.

RESULTS AND DISCUSSION

Characterization of Functionalized HNT. FTIR spectra (Figure 2) were obtained to confirm HNT modification. Compared to pristine HNTs, f-HNTs exhibited some new FTIR peaks, such as CH_2 stretching vibration bands (at 2933 and 2863 cm^{-1}) that were shifted to lower frequencies with respect to those observed for compound **1** (3060 and 2879 cm^{-1}), which is consistent with a compact packing of the organic moieties into the lumen.[24] The presence of the triazole ring in the f-HNTs was demonstrated by the stretching vibration bands of N═N and C—N aromatic groups around 1492 and 1376 cm^{-1}, respectively. Furthermore, f-HNTs did not show the stretching vibration bands of C≡C—H (2117 cm^{-1}) and N_3 (2063 cm^{-1}) groups, which were observed for compounds **1** and **2**, respectively.

The FTIR spectrum of f-HNTs was also characterized by the OH stretching vibrational bands of halloysite. The frequencies of these bands were not altered in the functionalized nanotubes. Specifically, we observed the broad peak of the water OH stretch as well as the OH stretching vibration bands of the Al—OH and Si—OH groups.

From these data, one can state that f-HNTs were synthesized. In addition, these findings were confirmed by TG studies (Figure 3).

In fact, f-HNTs exhibited typical halloysite weight losses occurring at ca. 550 and 750 °C attributed to the expulsion of interlayer water molecules and the dehydroxylation of alumina, respectively.[14] Moreover, the ratio between these weight losses was not altered by HNT functionalization.

The mass loss in the temperature range between 180 and 420 °C is due to the thermal degradation of the organic molecules incorporated in the HNT lumen. This degradation occurred in several steps as evidenced by the presence of two peaks (at ca. 250 and 350 °C) and a shoulder (at ca. 375 °C) in the differential thermogravimetric (DTG) curve. In addition, TG experiments allowed the degree of HNT functionalization to be determined as ca. 10 wt %. Based on the geometric volume of the nanotube cavity, it was reported[1] that ca. 10% of the void space is available for encapsulation. On this basis, we concluded that the organic molecules were incorporated into the HNT lumen with a high efficiency approaching the maximum expected loading.

Another confirmation of the functionalization of HNTs is provided by SEM (Figure 4), which indicates a fibrous

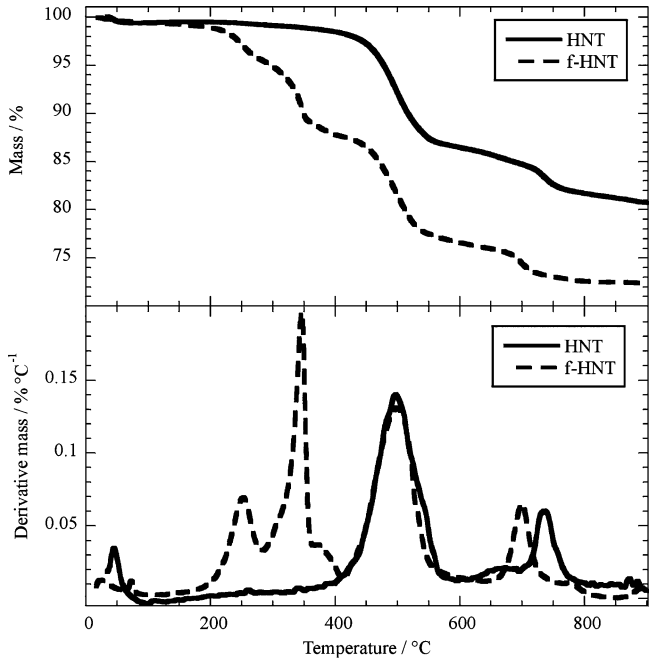

Figure 3. (Top) Thermogravimetric and (bottom) differential thermogravimetric curves of pristine and functionalized halloysite.

mesoscopic structure. The diameter of these fibers is ca. 14 μm, whereas the length ranges between 150 and 250 μm. Moreover, we observed the formation of anisotropic clusters with a size of ca. 200 μm. The surfaces of both the clusters and the fibers present randomly distributed nanotubes with sizes comparable to those of the pristine HNT sample.[14] These experiments indicated that the functionalization does not alter the tubular morphology of halloysite but it can generate organized structures in the micrometer range.

Characterization of Nanocomposite Films. Biocomposites films were successfully obtained with f-HNTs, and they evidenced macroscopic differences. The addition of the filler to both HPC and chitosan determined a decrease of the optical transparency (see Supporting Information). The chitosan/f-HNTs exhibited a surface much rougher than the pristine polymer, whereas this peculiarity was not observed for the chitosan/HNT hybrid. All films exhibit compact mechanical features.

dx.doi.org/10.1021/jp504388e | J. Phys. Chem. C XXXX, XXX, XXX−XXX

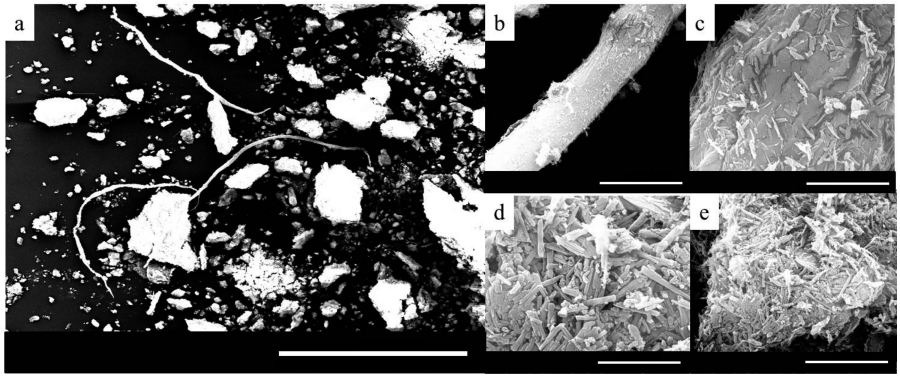

Figure 4. (a) SEM micrograph of functionalized halloysite (scale bar = 500 μm) and (b–e) high-magnification SEM micrographs of (b,c) microfibers (b, scale bar = 20 μm; c, scale bar = 5 μm) and (d,e) clusters (d, scale bar = 2 μm; e, scale bar = 5 μm) of functionalized halloysite.

Tensile Properties. We investigated the mechanical resistance to elongation for the prepared films by measuring the stress versus strain curves under a linear force ramp (some examples are reported in Figure 5). The tensile properties for

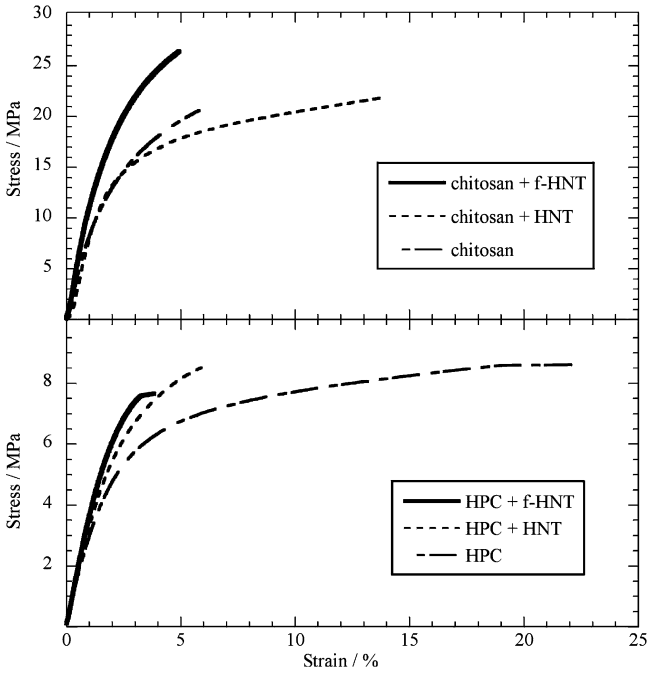

Figure 5. Stress vs strain curves for nanocomposite and polymer films.

pure biopolymers and nanocomposites are collected in Table 1. The performance of chitosan was found to be much better than that of HPC, in agreement with the presence of amino groups that enhance the interactions among the polymeric chains.

Regarding the nanocomposites, we found that the addition of f-HNTs generates films with better mechanical performance than for those based on pristine HNTs.

Filling the chitosan with small amounts of HNTs determined an increase in the elastic modulus (ca. 20%) in agreement with the literature.[25] The chitosan/f-HNT film exhibited the largest elastic modulus, with an improvement with respect to the pristine biopolymer of ca. 55%.

This extraordinary result was conferred by the microfibers of the functionalized nanotubes arranging themselves in a network with enhanced mechanical properties. It should be noted that

Table 1. Tensile Properties of Chitosan, HPC, and Their Nanocomposites[a]

film	elastic modulus (MPa)	stress at the breaking point (MPa)	elongation at the breaking point (%)	water contact angle (deg)
chitosan	820			75
chitosan/HNT	980			74
chitosan/f-HNT	1280			82
HPC	300	8.6	21.8	
HPC/HNT	320	8.5	6.1	
HPC/f-HNT	370	7.7	3.7	

[a]Relative errors are ±5% in elastic modulus, ±3% in stress and elongation at break, and ±1° in contact angle.

the stress at break for chitosan-based materials was not determined because it was outside the instrumental range.

For the HPC-based films, the presence of filler caused an enhancement of the elastic modulus (ca. 7% and ca. 23% for HNTs and f-HNTs, respectively), whereas the stress at the breaking point was slightly decreased. As Figure 5 shows, the elongation at the breaking point strongly decreased upon the addition of both pristine and functionalized nanotubes. This effect can be ascribed to the reduction of the sliding between the polymer chains against each other because of their interactions with the nanoclay,[22,26] which was also confirmed by the decrease of the elongation at break values (Table 1).

Morphology. The morphologies of the nanocomposites showed the effect of the filler on the mesoscopic structure of the films. For chitosan/HNTs, the surface appeared homogeneous, and the presence of nanotubes was rare (Figure 6).

On the contrary, the addition of f-HNTs to chitosan generated an increase in film roughness because of nanotube clusters (with a size of ca. 4 μm) that appeared on the surface (Figure 6). These results confirmed the enhancement of the surface hydrophobicity for the chitosan/f-HNT composite film. The variation of surface morphology is straightforwardly evidenced by the drop images collected just after the deposition of water drops and the corresponding contact angle values (Figure 6).

These results are intriguing because f-HNTs are hydrophilic in nature; moreover, the chitosan/HNT hybrid presents wettability behavior similar to that of the pristine biopolymer. Reports in the literature state that hydrophobic surfaces can be

dx.doi.org/10.1021/jp504388e | J. Phys. Chem. C XXXX, XXX, XXX–XXX

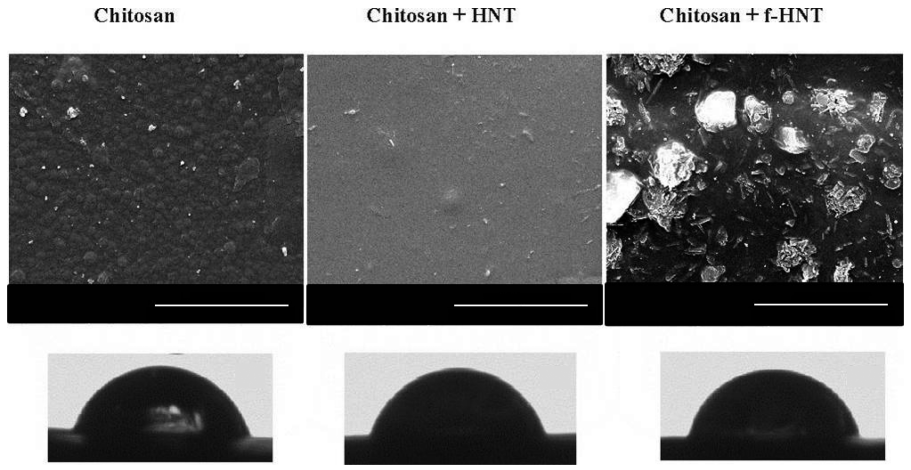

Figure 6. SEM micrographs and optical images of a water droplet just after the deposition of chitosan, chitosan/HNT, and chitosan/f-HNT films. Scale bars = 10 μm.

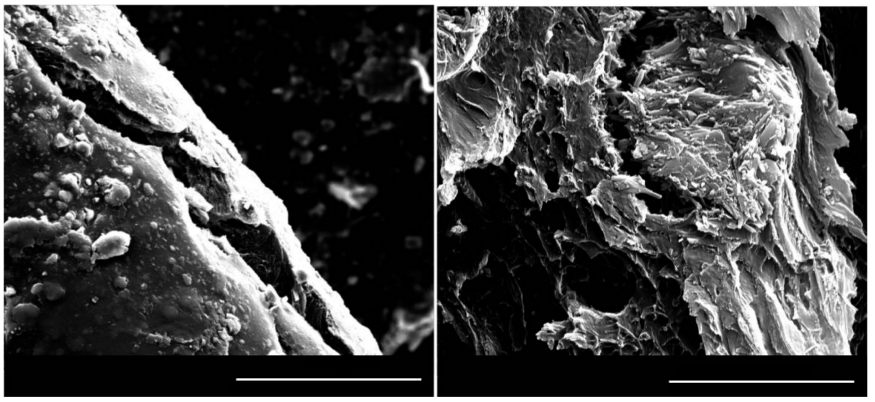

Figure 7. SEM micrographs of a transverse section of chitosan/f-HNT: scale bar = (left) 100 and (right) 5 μm.

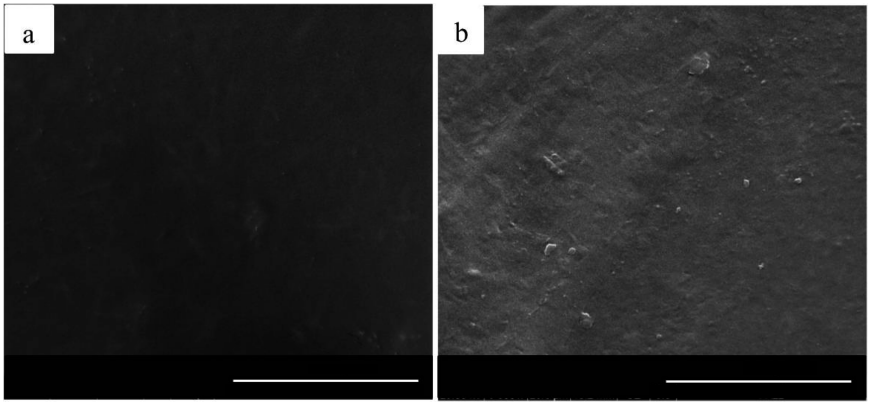

Figure 8. SEM micrographs of (a) HPC/HNT and (b) HPC/f-HNT. Scale bar = 10 μm.

generated by hydrophilic substances if a rough topography is induced.[27,28]

The formation of f-HNT clusters should generate a worsening of the film mechanical properties unless it is exclusively a surface phenomenon. To investigate the structure inside the films, SEM images of a transverse section of the chitosan/f-HNT nanocomposite were obtained (Figure 7).

We observed a multilayer structure with the presence of the f-HNT fibers along the thickness of the film and detected no clusters. Thus, one can conclude that the difference in morphology between the inner layers and the surface is responsible for the improvement of the mechanical performances.

As Figure 8 shows, both the HPC/HNT and HPC/f-HNT composite films presented smooth surfaces. The absence of nanotubes on the surface indicates that the filler was buried in the polymer matrix. Our previous work[18] demonstrated that, at high filler loadings, the addition of halloysite to the HPC matrix generates a sandwich-like structure in which the filler is segregated. This peculiarity was explained in terms of the low affinity between HNTs and HPC, which present hydrophilic and hydrophobic characters, respectively.

dx.doi.org/10.1021/jp504388e | J. Phys. Chem. C XXXX, XXX, XXX−XXX

The SEM insights indicated that f-HNTs do not favor polymer/filler interactions, as expected by the designed synthesis.

Thermal Degradation. Thermogravimetry is an appropriate technique for investigating the thermal degradation of both polymers and nanocomposites.[29−31]

Figure 9 shows that the pristine chitosan-based film thermally degrades in several steps.

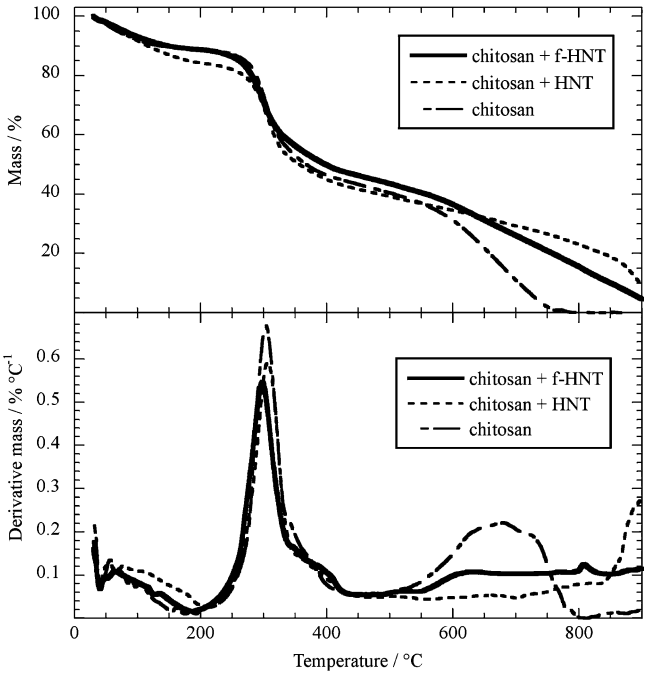

Figure 9. (Top) Thermogravimetric and (bottom) differential thermogravimetric curves of chitosan-based films.

The weight loss occurring from the ambient temperature to 150 °C was due to physically adsorbed water, whereas polymer degradation took place in two stages at higher temperature. The first stage started at ca. 220 °C and continued to ca. 420 °C, as evidenced by the sharp peak in the DTG curve. The second stage ranged between 500 and 800 °C, reaching a maximum degradation rate at ca. 675 °C. The broad peak in the DTG curve highlights that this degradation step was kinetically slower than the previous one.

The addition of the filler to the chitosan matrix influenced the polymer thermal stability. Compared to that of the pristine chitosan, the DTG peak reflecting the first stage of polymer degradation was shifted to higher and lower temperatures for HNTs and f-HNTs, respectively. Even though these variations were very small (within 5 °C), we can hypothesize that HNT functionalization reduces the barrier effect toward the mass transport of volatile products because the lumen is occupied by organic molecules. This interpretation is corroborated by the TG data relative to the second step of the chitosan degradation; accordingly, f-HNTs did not influence the temperature range, whereas HNTs strongly enhanced the polymer resistance to the thermal degradation (the process started at ca. 850 °C).

Regarding the HPC-based films, we observed that both the pristine polymer and the nanocomposites thermally degraded into two steps (Figure 10). All systems presented a first weight loss of ca. 4 wt % in the temperature range between 25 and 150 °C that is correlated to the water content of the materials.

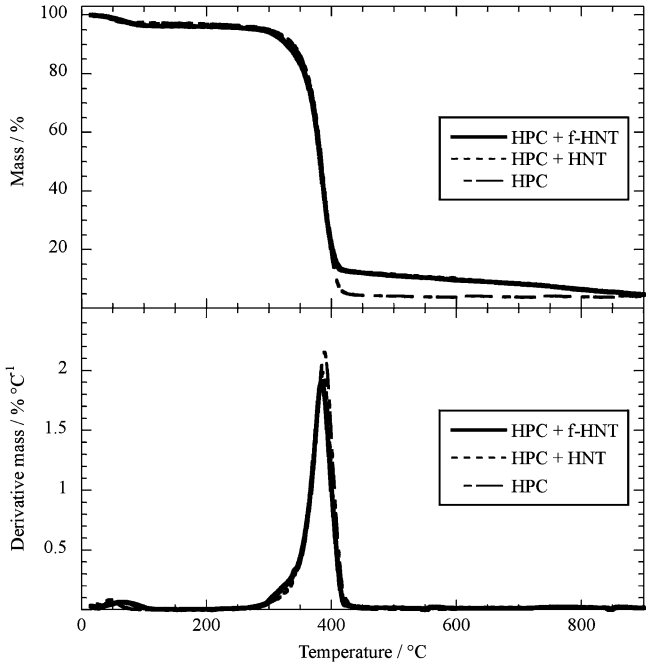

Figure 10. (Top) Thermogravimetric and (bottom) differential thermogravimetric curves of HPC-based films.

Polymer degradation occurred in one stage in the interval from 250 to 450 °C. The effect of the filler on the HPC thermal stability was negligible, as the degradation maximum rate slowly shifted to lower temperatures (the variations are within 4 °C). These results agree with the morphological insights that evidenced a low affinity between the polymer and the nanoparticles.

■ CONCLUSIONS

Functionalization of the inner lumen of halloysite nanotubes by means of the click reaction involving azides and alkynes was achieved. The synthesis of the modified HNTs was successful as confirmed by thermogravimetry and IR spectroscopy. SEM investigations showed the presence of fibers and clusters in the micrometer range. Nanocomposite films based on both pristine and modified halloysite were prepared. The fillers were dispersed into chitosan and hydroxypropyl cellulose. A comprehensive physicochemical study of the bionanomaterials was carried out through wettability, thermal degradation, and tensile properties, which were correlated with the mesoscopic structure. Bionanocomposites based on the functionalized nanotubes and chitosan presented a strong enhancement in the mechanical performances as a result of the presence of fibers of HNTs. Furthermore, the surface presence of modified HNT clusters enhanced the surface roughness, leading to an increase in the water contact angle. Less relevant effects were observed for the nanocomposite based on hydroxypropyl cellulose.

With this study, we successfully propose a selective reaction of the halloysite inner cavity to obtain microfibers that can be used as green fillers to reinforce biopolymeric materials. The structural and surface properties are tunable, and therefore, a variety of materials with controlled behavior can be obtained.

dx.doi.org/10.1021/jp504388e | J. Phys. Chem. C XXXX, XXX, XXX−XXX

■ ASSOCIATED CONTENT

Supporting Information

Details on the synthesis. Optical photographs of the biofilms. This material is available free of charge via the Internet at http://pubs.acs.org.

■ AUTHOR INFORMATION

Corresponding Authors

*Phone: +39 09123897962. E-mail: giuseppe.lazzara@unipa.it.
*Phone: +39 09123897546. E-mail: serena.riela@unipa.it.

Notes

The authors declare no competing financial interest.

■ ACKNOWLEDGMENTS

The work was financially supported by the University of Palermo, PRIN 2010-2011 (prot. 2010329WPF) and FIRB 2012 (prot. RBFR12ETL5).

■ REFERENCES

(1) Lvov, Y.; Abdullayev, E. Functional Polymer−Clay Nanotube Composites with Sustained Release of Chemical Agents. *Prog. Polym. Sci.* **2013**, *38*, 1690−1719.

(2) Lvov, Y. M.; Shchukin, D. G.; Mohwald, H.; Price, R. R. Halloysite Clay Nanotubes for Controlled Release of Protective Agents. *ACS Nano* **2008**, *2*, 814−820.

(3) Barrientos-Ramírez, S.; Ramos-Fernández, E. V.; Silvestre-Albero, J.; Sepúlveda-Escribano, A.; Pastor-Blas, M. M.; González-Montiel, A. Use of Nanotubes of Natural Halloysite as Catalyst Support in the Atom Transfer Radical Polymerization of Methyl Methacrylate. *Microporous Mesoporous Mater.* **2009**, *120*, 132−140.

(4) Massaro, M.; Riela, S.; Cavallaro, G.; Gruttadauria, M.; Milioto, S.; Noto, R.; Lazzara, G. Eco-Friendly Functionalization of Natural Halloysite Clay Nanotube with Ionic Liquids by Microwave Irradiation for Suzuki Coupling Reaction. *J. Organomet. Chem.* **2014**, *749*, 410−415.

(5) Machado, G. S.; de Freitas Castro, K. A. D.; Wypych, F.; Nakagaki, S. Immobilization of Metalloporphyrins into Nanotubes of Natural Halloysite toward Selective Catalysts for Oxidation Reactions. *J. Mol. Catal. Chem.* **2008**, *283*, 99−107.

(6) Wang, R.; Jiang, G.; Ding, Y.; Wang, Y.; Sun, X.; Wang, X.; Chen, W. Photocatalytic Activity of Heterostructures Based on TiO_2 and Halloysite Nanotubes. *ACS Appl. Mater. Interfaces* **2011**, *3*, 4154−4158.

(7) Zhao, Y.; Abdullayev, E.; Vasiliev, A.; Lvov, Y. Halloysite Nanotubule Clay for Efficient Water Purification. *J. Colloid Interface Sci.* **2013**, *406*, 121−129.

(8) Luo, P.; Zhao, Y.; Zhang, B.; Liu, J.; Yang, Y.; Liu, J. Study on the Adsorption of Neutral Red from Aqueous Solution onto Halloysite Nanotubes. *Water Res.* **2010**, *44*, 1489−1497.

(9) Abdullayev, E.; Sakakibara, K.; Okamoto, K.; Wei, W.; Ariga, K.; Lvov, Y. Natural Tubule Clay Template Synthesis of Silver Nanorods for Antibacterial Composite Coating. *ACS Appl. Mater. Interfaces* **2011**, *3*, 4040−4046.

(10) Wei, W.; Minullina, R.; Abdullayev, E.; Fakhrullin, R.; Mills, D.; Lvov, Y. Enhanced Efficiency of Antiseptics with Sustained Release from Clay Nanotubes. *RSC Adv.* **2014**, *4*, 488−494.

(11) Abdullayev, E.; Lvov, Y. Clay Nanotubes for Corrosion Inhibitor Encapsulation: Release Control with End Stoppers. *J. Mater. Chem.* **2010**, *20*, 6681−6687.

(12) Shchukin, D. G.; Möhwald, H. Self-Repairing Coatings Containing Active Nanoreservoirs. *Small* **2007**, *3*, 926−943.

(13) Cavallaro, G.; Donato, D. I.; Lazzara, G.; Milioto, S. Films of Halloysite Nanotubes Sandwiched between Two Layers of Biopolymer: From the Morphology to the Dielectric, Thermal, Transparency, and Wettability Properties. *J. Phys. Chem. C* **2011**, *115*, 20491−20498.

(14) Cavallaro, G.; Lazzara, G.; Milioto, S. Dispersions of Nanoclays of Different Shapes into Aqueous and Solid Biopolymeric Matrices. Extended Physicochemical Study. *Langmuir* **2011**, *27*, 1158−1167.

(15) Du, M.; Guo, B.; Jia, D. Thermal Stability and Flame Retardant Effects of Halloysite Nanotubes on Poly(propylene). *Eur. Polym. J.* **2006**, *42*, 1362−1369.

(16) Liu, M.; Wu, C.; Jiao, Y.; Xiong, S.; Zhou, C. Chitosan−Halloysite Nanotubes Nanocomposite Scaffolds for Tissue Engineering. *J. Mater. Chem. B* **2013**, *1*, 2078−2089.

(17) Luo, Z.; Song, H.; Feng, X.; Run, M.; Cui, H.; Wu, L.; Gao, J.; Wang, Z. Liquid Crystalline Phase Behavior and Sol−Gel Transition in Aqueous Halloysite Nanotube Dispersions. *Langmuir* **2013**, *29*, 12358−12366.

(18) Cavallaro, G.; Lazzara, G.; Milioto, S. Exploiting the Colloidal Stability and Solubilization Ability of Clay Nanotubes/Ionic Surfactant Hybrid Nanomaterials. *J. Phys. Chem. C* **2012**, *116*, 21932−21938.

(19) Yah, W. O.; Takahara, A.; Lvov, Y. M. Selective Modification of Halloysite Lumen with Octadecylphosphonic Acid: New Inorganic Tubular Micelle. *J. Am. Chem. Soc.* **2011**, *134*, 1853−1859.

(20) Zheng, Y.; Wang, A. Enhanced Adsorption of Ammonium Using Hydrogel Composites Based on Chitosan and Halloysite. *J. Macromol. Sci. A* **2009**, *47*, 33−38.

(21) Prashantha, K.; Schmitt, H.; Lacrampe, M. F.; Krawczak, P. Mechanical Behaviour and Essential Work of Fracture of Halloysite Nanotubes Filled Polyamide 6 Nanocomposites. *Compos. Sci. Technol.* **2011**, *71*, 1859−1866.

(22) Cavallaro, G.; Lazzara, G.; Milioto, S. Sustainable Nanocomposites Based on Halloysite Nanotubes and Pectin/Polyethylene Glycol Blend. *Polym. Degrad. Stab.* **2013**, *98*, 2529−2536.

(23) Wang, Q.; Xie, X.; Zhang, X.; Zhang, J.; Wang, A. Preparation and Swelling Properties of pH-Sensitive Composite Hydrogel Beads Based on Chitosan-*g*-Poly(acrylic Acid)/Vermiculite and Sodium Alginate for Diclofenac Controlled Release. *Int. J. Biol. Macromol.* **2010**, *46*, 356−362.

(24) Zhu, J.; He, H.; Zhu, L.; Wen, X.; Deng, F. Characterization of Organic Phases in the Interlayer of Montmorillonite Using FTIR and ^{13}C NMR. *J. Colloid Interface Sci.* **2005**, *286*, 239−244.

(25) Liu, M.; Zhang, Y.; Wu, C.; Xiong, S.; Zhou, C. Chitosan/Halloysite Nanotubes Bionanocomposites: Structure, Mechanical Properties and Biocompatibility. *Int. J. Biol. Macromol.* **2012**, *51*, 566−575.

(26) Tang, X.; Alavi, S. Structure and Physical Properties of Starch/Poly Vinyl Alcohol/Laponite RD Nanocomposite Films. *J. Agric. Food Chem.* **2012**, *60*, 1954−1962.

(27) Marmur, A. From Hygrophilic to Superhygrophobic: Theoretical Conditions for Making High-Contact-Angle Surfaces from Low-Contact-Angle Materials. *Langmuir* **2008**, *24*, 7573−7579.

(28) Liu, M.; Jia, Z.; Liu, F.; Jia, D.; Guo, B. Tailoring the Wettability of Polypropylene Surfaces with Halloysite Nanotubes. *J. Colloid Interface Sci.* **2010**, *350*, 186−193.

(29) Blanco, I.; Abate, L.; Bottino, F. A.; Bottino, P. Thermal Degradation of Hepta Cyclopentyl, Mono Phenyl-Polyhedral Oligomeric Silsesquioxane (hcp-POSS)/Polystyrene (PS) Nanocomposites. *Polym. Degrad. Stab.* **2012**, *97*, 849−855.

(30) Rotaru, A.; Nicolaescu, I.; Rotaru, P.; Neaga, C. Thermal Characterization of Humic Acids and Other Components of Raw Coal. *J. Therm. Anal. Calorim.* **2008**, *92*, 297−300.

(31) Duce, C.; Ghezzi, L.; Onor, M.; Bonaduce, I.; Colombini, M.; Tinè, M.; Bramanti, E. Physico-Chemical Characterization of Protein−Pigment Interactions in Tempera Paint Reconstructions: Casein/Cinnabar and Albumin/Cinnabar. *Anal. Bioanal. Chem.* **2012**, *402*, 2183−2193.